Progress In Electromagnetics Research, PIER 93, 161–176, 2009

A NEW MICROWAVE METHOD BASED ON TRANSMISSION SCATTERING PARAMETER MEASUREMENTS FOR SIMULTANEOUS BROADBAND AND STABLE PERMITTIVITY AND PERMEABILITY DETERMINATION

U. C. Hasar †

Department of Electrical and Electronics Engineering
Ataturk University
Erzurum 25240, Turkey

Abstract—A new microwave method has been proposed for simultaneous broadband and stable complex permittivity and complex permeability determination of magnetic and nonmagnetic materials. The method utilizes complex transmission scattering measurements at different frequencies. For a change in constitutive parameters determination, we considered zero-order and higher-order approximations. We have verified the proposed method from measurements of two medium- and low-loss materials with another method and available reference data in the literature.

1. INTRODUCTION

Various microwave methods have been proposed in materials characterization regime [1–3]. While resonant methods have better accuracy and sensitivity, nonresonant methods are broadband and require less sample preparation. Due to its relative simplicity, transmission/reflection (TR) nonresonant methods are most widely used [4, 5].

For broadband complex permittivity, ε, and complex permeability, μ, determination of materials from complex scattering (S-) parameter measurements (S_{11} and S_{21}), the Nicolson-Ross-Weir (NRW) technique [6, 7] has been widely used over 30 years. Because initially this technique was considered for a three-layer structure, a modification has been made to suit it for granular and liquid materials plugged

Corresponding author: U. C. Hasar (ugurcem@atauni.edu.tr).
† Also with Department of Electrical and Computer Engineering, Binghamton University, Binghamton, NY 13902, USA.

(or sandwiched) by two low-loss materials [8] and for high-loss thin materials backed by a low-loss material which is used solely for holding thin materials [9]. It is well-known that derived equations for ε and μ in the NRW technique and its extended versions briefly discussed above [6–9] will become algebraically unstable when S_{11} approaches zero. This is a general case for low-loss materials. In order to resolve this problem, firstly Baker-Jarvis et al. applied an iterative technique using the value of a constant, β, in the iteration [10]. Then, Huashen et al. proposed a new NRW transmission/reflection algorithm for the same problem [11]. In addition, Varadan and Ro have recently proposed a technique, which uses Kramers-Kronig relations between the measured attenuation and phase constants [12]. While the former is utilized to measure only the ε, the latter two can extract both the ε and μ. However, for magnetic low-loss materials, all these methods suffer from the problem of undesired ripples in simultaneous ε and μ measurements when the thickness of these materials is a multiple of half-wavelengths. This arises as a result of enormously increased uncertainty in the phase of reflection S-parameters. Boughriet et al. introduced an effective ε and μ concept of materials for solving the ripples problem [13]. They stated that the ill-natured term responsible for breaking down of the NRW technique for low-loss materials is $1 - \Gamma/1 + \Gamma$. We also proposed new methodologies (amplitude-based measurement techniques) to remove the same problem [14–16]. However, none of these methods can non-ambiguously and simultaneously measure the ε and μ of magnetic materials.

A promising solution to the original problem (simultaneous ε and μ determination for medium- and low-loss materials) can pass through using transmission-only complex S-parameter measurements. In addition that these measurements do not have any phase uncertainty problems for low- and medium-loss materials, they have as well two more advantageous over reflection-only complex S-parameter measurements as: 1) They provide longitudinal averaging of variations in sample properties [17] and 2) their spectral integrity experiences less deterioration from surface roughness at high frequencies [18, 19]. Transmission measurements of two samples with same electrical and internal properties but different lengths can be employed as a remedy for simultaneous ε and μ determination [5]. However, this approach (will be denoted as varying thickness method in the remaining of the manuscript) may become unstable for low-loss materials if the sample lengths simultaneously resonate at certain frequencies [5]. In addition, any inaccuracy in the second sample thickness can degrade the overall measurement accuracy. To increase the correctness of measurements, obtain a stable solution, and eliminate the undesired

peaks in simultaneous ε and μ measurements of low-loss materials, in this study, we present a different formulation, which accommodates transmission-only complex S-parameter measurements at separated frequencies.

The organization of the paper is as follows. First, in Section 2, we present a theoretical background for the proposed method. Next, in Section 3, we derive an objective function for simultaneous and stable ε and μ determination from S_{21} parameter measurements. Finally, for validation of the proposed method, in Section 4, X-band measurements of ε and μ of two medium- and low-loss samples fitted tightly into a waveguide section by the proposed method and by the varying thickness method are compared.

2. THEORETICAL BACKGROUND

A typical problem for the ε and μ determination of a sample with length L in a waveguide is shown in Fig. 1. It is assumed that the sample is isotropic, homogenous, flat, and tightly fitted to its holder (a waveguide section). Also, we assume that the waveguide operates at the dominant mode (TE_{10}).

Using vector potentials for electromagnetic fields and applying boundary conditions at end surfaces of the sample and at inner waveguide walls, S-parameters at sample surfaces can be obtained [4, 5] as

$$S_{11} = |S_{11}|e^{j\theta_{11}} = \Gamma\frac{(1-T^2)}{1-\Gamma^2T^2}, \quad S_{21} = |S_{21}|e^{j\theta_{21}} = T\frac{(1-\Gamma^2)}{1-\Gamma^2T^2}, \quad (1)$$

where $|\cdot|$ denotes the magnitude of expressions and Γ and T are, respectively, the reflection coefficient when the sample is semi-infinite in length and the propagation factor. Their corresponding equations

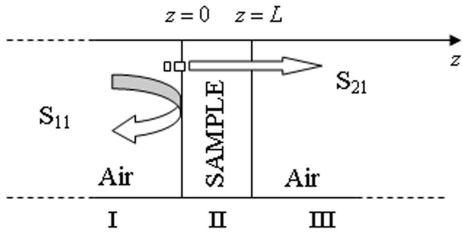

Figure 1. The configuration for S-parameter measurements in a waveguide.

are

$$\Gamma = \frac{Z - Z_0}{Z + Z_0},\ T = \exp(-\gamma L),\ \gamma = \mathrm{i}\frac{2\pi}{\lambda_0}\sqrt{\varepsilon\mu - (\lambda_0/\lambda_c)^2} \tag{2}$$

$$\gamma_0 = \mathrm{i}\frac{2\pi}{\lambda_0}\sqrt{1 - (\lambda_0/\lambda_c)^2},\ Z = \mathrm{i}\frac{\omega\mu_0\mu}{\gamma},\ Z_0 = \mathrm{i}\frac{\omega\mu_0}{\gamma_0},$$
$$\varepsilon = \varepsilon' - \mathrm{i}\varepsilon'',\ \mu = \mu' - \mathrm{i}\mu''. \tag{3}$$

Here, γ_0, Z_0, and γ, Z, represent, respectively, the propagation constants and the impedances of empty- and the sample-filled cells; $\lambda_0 = c/f$ and $\lambda_c = c/f_c$ correspond to the free-space and cut-off wavelengths; and f and f_c are the operating and cut-off frequencies.

3. NEW FORMULATION

3.1. Ill-natured Behaviour of Reflection Measurements

To fully understand the efficiency of new formulation, it is important to analyze the behaviour of S_{11} and S_{21} at frequencies where L is of integer multiples of one-half guided wavelength, λ_g. We firstly investigated the behaviours of $|S_{11}|$ and $|S_{21}|$ at those frequencies. We expressed γ in (2)

$$\gamma = \alpha + j\beta = j\frac{2\pi}{\lambda_0}\sqrt{\varepsilon\mu - (\lambda_0/\lambda_c)^2}, \tag{4}$$

where α and β are, respectively, the attenuation and phase constants. Taking the square of both sides in (4) and then expressing it in terms of β yields an expression as

$$\beta^4 - \frac{2\pi}{\lambda_0}(\varepsilon'\mu' - \varepsilon''\mu'' - (\lambda_0/\lambda_c)^2)\beta^2 - \left[\frac{2\pi}{\lambda_0}(\varepsilon'\mu'' + \varepsilon''\mu')\right]^2 = 0. \tag{5}$$

Using (5), the roots of β will be

$$\beta_{(1,2)} = \frac{2\pi}{\lambda_0}\left[\frac{\varepsilon'\mu' - \varepsilon''\mu'' - (\lambda_0/\lambda_c)^2 \mp \sqrt{\left(\varepsilon'\mu' - \varepsilon''\mu'' - (\lambda_0/\lambda_c)^2\right)^2 + (\varepsilon'\mu'' + \varepsilon''\mu')^2}}{2}\right]^{1/2}, \tag{6}$$

The correct root for β in (6) can easily be identified by using the fact that $\beta > 0$. It is apparent that the sum of the terms in the square root in (6) must be greater than that of the terms just outside it for $\beta > 0$. As a result, the correct root for β will be when the sign before the square root in (6) is positive. Then, α will be

$$\alpha = 2\left(\frac{\pi}{\lambda_0}\right)^2 \frac{(\varepsilon'\mu'' + \varepsilon''\mu')}{\beta}. \tag{7}$$

When $L \cong n\lambda_g/2$ where n is a positive integer, we can approximate β and T^2 in (2) as

$$\beta \cong n\pi/L, \quad T^2 \cong e^{-2\alpha L} = e^{-\left(\frac{2L}{\lambda_0}\right)^2 \frac{(\varepsilon''\mu'+\varepsilon'\mu'')}{n}\pi}. \tag{8}$$

It is obvious from (8) that T^2 approaches one when ε'' and μ'' simultaneously go to zero, which is a typical case for low-loss dielectric materials ($\mu = 1$). In this circumstance, it is obvious from (1) that $|S_{11}|$ shrinks to zero while $|S_{21}|$ goes to one. When the sample becomes lossless ($\varepsilon'' \approx 0$ and $\mu'' \approx 0$) or low-loss ($\varepsilon'' \ll \varepsilon'$ and $\mu'' \ll \mu'$), the electromagnetic waves will attenuate less. In this condition, it is obvious from (7) that α approaches zero. When $\alpha \cong 0$, the expression for β in (7) seems to have an instability (0/0). Because, in the manuscript, our purpose is to investigate what happens to T^2 when $L \cong n\lambda_g/2$, we directly substitute that specific case into the expression for T^2. It is obvious from (8) that $\beta \cong n\pi/L$. This clearly verifies that β is a parameter greater than one for samples with a moderate length ($L < 1$ m), which is a general case for measurements in materials characterization, since $n = 1, 2, 3, \ldots$.

We next analyze θ_{11} and θ_{21} in (1) and define new variables for this purpose as

$$\begin{aligned} &\chi - j\xi = \sqrt{\varepsilon\mu - (\lambda_0/\lambda_c)^2}, \quad B = \exp\left(-\tfrac{4\pi}{\lambda_0}\xi L\right), \\ &A = \tfrac{4\pi}{\lambda_0}\chi L, \quad \sigma - j\tau = \mu\sqrt{1 - (\lambda_0/\lambda_c)^2}. \end{aligned} \tag{9}$$

Using (9), we express θ_{11} and θ_{21} in terms of new variables as

$$\begin{aligned} \theta_{11} = {} & \arctan\left(\frac{\Omega_1 B\sin(A) - \Omega_2\left(1 - B\cos(A)\right)}{\Omega_1\left(1 - B\cos(A)\right) + \Omega_2 B\sin(A)}\right) \\ & - \arctan\left(\frac{\Omega_4 B\cos(A) - \Omega_6 + \Omega_3 B\sin(A)}{\Omega_4 B\sin(A) + \Omega_5 - \Omega_3 B\cos(A)}\right) \mp 2\pi n, \end{aligned} \tag{10}$$

$$\begin{aligned} \theta_{21} = {} & -\frac{A}{2} - \arctan\left(\frac{\sigma\xi + \tau\chi}{\sigma\chi - \tau\xi}\right) \\ & - \arctan\left(\frac{\Omega_4 B\cos(A) - \Omega_6 + \Omega_3 B\sin(A)}{\Omega_4 B\sin(A) + \Omega_5 - \Omega_3 B\cos(A)}\right) \mp 2\pi m, \end{aligned} \tag{11}$$

where m and n are integers and

$$\begin{aligned} &\Omega_1 = \sigma^2 - \chi^2 + \xi^2 - \tau^2, \quad \Omega_2 = 2\left(\sigma\tau - \chi\xi\right), \\ &\Omega_3 = \left(\sigma - \chi\right)^2 - \left(\tau - \xi\right)^2, \quad \Omega_4 = 2\left(\sigma - \chi\right)\left(\tau - \xi\right), \\ &\Omega_5 = \left(\sigma + \chi\right)^2 - \left(\tau + \xi\right)^2, \quad \Omega_6 = 2\left(\sigma + \chi\right)\left(\tau + \xi\right). \end{aligned} \tag{12}$$

We perform a numerical analysis to understand the behaviour of each term in θ_{11} and θ_{21}. For example, Fig. 2 illustrates the

dependency of θ_{11}, the first and second phase terms ($\arctan(\Omega_1, \Omega_2)$ and $\arctan(\Omega_3, \Omega_4, \Omega_5, \Omega_6)$) in (10), and $|S_{11}|$ over f for $\varepsilon = 12.6 - \mathrm{i}0.02$, $\mu = 1 - \mathrm{i}0.02$, f_c=6.555 GHz, and L=20 mm. In this figure, while θ_{11}, $\arctan(\Omega_1, \Omega_2)$ and $\arctan(\Omega_3, \Omega_4, \Omega_5, \Omega_6)$ are given in radians, $|S_{11}|$ is given in linear format.

It is clearly seen from Fig. 2 that the linearity of θ_{11} over f deteriorates when $|S_{11}|$ gets maximum or minimum. In addition, we note that the dependency of θ_{11} shows a deflection when $|S_{11}|$ approaches minimum, e.g., $f \cong 8.6$ GHz. It is also seen that while $\arctan(\Omega_1, \Omega_2)$ follows the same pattern of θ_{11} over f, $\arctan(\Omega_3, \Omega_4, \Omega_5, \Omega_6)$ shrinks to zero when $|S_{11}|$ is minimum or maximum. Because it is known that the ripples seen in the measured ε and μ are similar to those of θ_{11} in Fig. 2, we conclude that the ripples in measured ε and μ can come from $\arctan(\Omega_1, \Omega_2)$. To support this conclusion, we drew other dependencies of θ_{11}, $\arctan(\Omega_1, \Omega_2)$, $\arctan(\Omega_3, \Omega_4, \Omega_5, \Omega_6)$, and $|S_{11}|$ over f for different ε, μ, f_c, and L where $\varepsilon'' \ll \varepsilon'$ and $\mu'' \ll \mu'$ (low-loss magnetic materials). We observed similar behaviours as given in Fig. 2.

We also analyzed the dependency of θ_{21}. For instance, Fig. 3 shows the dependency of θ_{21}, the first and second phase terms ($A/2$ and $\arctan(\chi, \xi, \sigma, \tau)$) in (11), and $|S_{21}|$ for the same test parameters in Fig. 2. Because the third phase term of θ_{21} in (11) is the same as of the second term of θ_{11}, that term is not analyzed here. It is clear from Fig. 3 that the first phase term in (11) follows the dependency of θ_{21} over f, and its linearity does not show any deflection and/or change at frequencies which result in maximum and/or minimum $|S_{21}|$. In

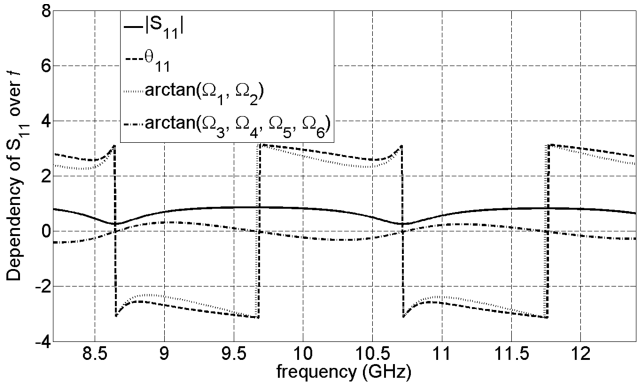

Figure 2. Dependency of $|S_{11}|$, θ_{11}, and the first and second phase terms ($\arctan(\Omega_1, \Omega_2)$ and $\arctan(\Omega_3, \Omega_4, \Omega_5, \Omega_6)$) in (10) for $\varepsilon = 12.6 - \mathrm{i}0.02$, $\mu = 1 - \mathrm{i}0.02$, $f_c = 6.555$ GHz, and L=20 mm.

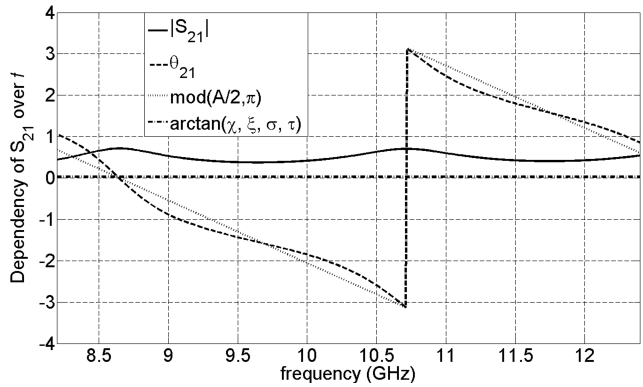

Figure 3. Dependency of $|S_{21}|$, θ_{21}, the first and second phase terms ($A/2$ and $\arctan(\chi, \xi, \sigma, \tau)$) in (11) for $\varepsilon = 12.6 - \mathrm{i}0.02$, $\mu = 1 - \mathrm{i}0.02$, $f_c = 6.555\,\mathrm{GHz}$, and $L = 20\,\mathrm{mm}$.

addition, the second phase term of θ_{21} in (11) is approximately zero for $\varepsilon'' \ll \varepsilon'$ and $\mu'' \ll \mu'$, and can be assumed stable over f. From these data, we conclude that all these phase terms in (11) can be assumed stable and will not produce any peaks in the extracted ε and μ over a wide frequency band. These results are totally in good agreement with the measurement results in the literature.

3.2. Mathematical Analysis

In previous section, we demonstrated that the first phase term in (10) is responsible for the peaks in the extracted ε and μ. In this section, we will present a new formulation, which is based upon using S_{21} parameter measurements at separated frequencies, for simultaneous and stable ε and μ extraction of materials, and thus eliminate the undesired effect of the first phase term in (10) on measurements. Because electrical properties of materials could slightly or largely change with frequency depending on its internal properties, we will analyze two approximations to simulate this change.

3.2.1. Zero-order (ZO) Approximation

This approximation assumes that $f_2 = f \mp \Delta f = \mathrm{u}f$ where $\Delta f > 0$, $\Delta f \ll f$, and u is a constant [16, 20, 21]. Using this condition, we can approximate $\varepsilon \approx \varepsilon(f_2)$ and $\mu \approx \mu(f_2)$. It is obvious from (1)–(3) that measured $S_{21}(f_2)$ will not be equal to measured S_{21} since the frequency

changes. Then, we can write

$$\Gamma(f_2) \approx \frac{\sqrt{1-(\lambda_0 \mathrm{u}\lambda_c)^2}\mu - \sqrt{\varepsilon\mu-(\lambda_0 \mathrm{u}\lambda_c)^2}}{\sqrt{1-(\lambda_0 \mathrm{u}\lambda_c)^2}\mu + \sqrt{\varepsilon\mu-(\lambda_0 \mathrm{u}\lambda_c)^2}},$$
$$T(f_2) \approx \exp\left(-\mathrm{iu}\tfrac{2\pi}{\lambda_0} L\sqrt{\varepsilon\mu-(\lambda_0 \mathrm{u}\lambda_c)^2}\right). \quad (13)$$

We further assume that $(\lambda_0/\mathrm{u}\lambda_c)^2 \approx (\lambda_0\lambda_c)^2$ (which is truly the case for coaxial-line measurements) in (13) since $\Delta f \ll f$. Using this assumption, we can write

$$\Gamma(f_2) \cong \Gamma, \qquad T(f_2) \cong T^{\mathrm{u}}. \quad (14)$$

Next, using (1), we can express T in terms of Γ as

$$T_{(1,2)} = -\left(\frac{1}{S_{21}}\frac{\left(1-\Gamma^2\right)}{\Gamma^2} \mp \sqrt{\Delta_T}\right)/2,\ \Delta_T = \frac{\left(1-\Gamma^2\right)^2}{S_{21}^2\Gamma^4} + \frac{4}{\Gamma^2}. \quad (15)$$

In a similar manner, we express $T(f_2)$ in terms of $\Gamma(f_2)$ in a similar form between T and Γ in (15). Finally, using (14), $T(f_2)$, and $\Gamma(f_2)$, we derive an objective function for determination of Γ as

$$F_{obj} = \left[\frac{-\frac{\left(1-\Gamma^2\right)}{S_{21}\Gamma^2} \mp \sqrt{\frac{\left(1-\Gamma^2\right)^2}{S_{21}^2\Gamma^4} + \frac{4}{\Gamma^2}}}{2}\right]^{\mathrm{u}}$$
$$- \left[\frac{-\frac{\left(1-\Gamma^2(f_2)\right)}{S_{21}(f_2)\Gamma^2(f_2)} \mp \sqrt{\frac{\left(1-\Gamma^2(f_2)\right)^2}{S_{21}^2(f_2)\Gamma^4(f_2)} + \frac{4}{\Gamma^2(f_2)}}}{2}\right] \cong 0, \quad (16)$$

where it is assumed that $\Gamma \cong \Gamma(f_2)$. It is obvious from (16) that the derived objective function is similar to that obtained from S_{21} measurements of two identical samples with different lengths [5]. However, in this paper, we utilize a different approach, which not only eliminates errors arising from any sample inhomogeneity and irregularity inside the second sample but also yields a stable and dynamic extraction of ε and μ, for low-loss magnetic and nonmagnetic materials.

The Newton's search algorithm can be applied to (16) with the constrain that $|\Gamma| \ll 1$ [22]. After computing Γ, we can find T and $T(f_2)$ by using (15) and (14), respectively. At the end, ε and μ can be

determined by

$$\frac{1}{\Lambda^2} = \left[\frac{\mathrm{i}}{2\pi L}\ln(T)\right]^2,\ \mu = \frac{(1+\Gamma)}{(1-\Gamma)}\frac{1}{\Lambda\sqrt{\frac{1}{\lambda_0^2}-\frac{1}{\lambda_c^2}}}, \tag{17}$$

$$\varepsilon = \frac{1}{\mu}\left[\left(\frac{\lambda_0}{\Lambda}\right)^2 + \left(\frac{\lambda_0}{\lambda_c}\right)^2\right]. \tag{18}$$

At this point, we have to discuss about the term $1+\Gamma/1-\Gamma$ in (17). It was concluded that this term was the term which produces the undesired peaks in simultaneous ε and μ extraction using reflection and transmission measurements [13]. Although we also use this term for μ determination in (17), our extracted ε and μ will not experience any unexpected peaks since this term in our equations is not a function of reflection measurements. In other words, the main reason for observing ripples in the extracted ε and μ from NRW technique is that Γ significantly increases when S_{11} approaches zero. Any incorrect measurement of the phase or the amplitude of S_{11} near frequencies which produce thickness resonance effect will drastically affect the measured Γ. This in turn will generate ripples in measured ε and μ.

3.2.2. Higher-order (HO) Approximations

If S_{21} measurements at two frequencies do not much change, then we should search for new frequencies that yield different S_{21} values. However, using S_{21} measurements at widely separated frequencies may not suit the ZO approximation since ε and μ can change considerably. In this circumstance, higher-order (HO) approximations should be adapted. These approximations consider cases where $\varepsilon \neq \varepsilon(f_2)$ and $\mu \neq \mu(f_2)$ as well as $\varepsilon \approx \varepsilon(f_2)$ and $\mu \approx \mu(f_2)$ over small frequency shifts, $\Delta f \ll 1$. For these approximations, ε and μ can suitably be expressed as [16, 23, 24]

$$\varepsilon(f) = \sum_{n=0}^{m} C_n f^n = C_0 + C_1 f + C_2 f^2 + C_3 f^3 + \ldots \tag{19}$$

$$\mu(f) = \sum_{n=0}^{m} D_n f^n = D_0 + D_1 f + D_2 f^2 + D_3 f^3 + \ldots, \tag{20}$$

where C_n's and D_n's are the unknown complex quantities and 'm' is the degree of power, which should be selected according to the properties of materials. It is clear that for $m = 0$, 1, and 2, the expressions in (19) and (20) will reduce to zero-order [16, 20, 21], first-order [24],

and second-order [23] approximations, respectively. To apply HO approximations for simultaneous ε and μ extraction, the well-known least squares minimization algorithm can be applied [22] given as

$$\min \left\| \sum S_{21}(f) - P_{21}(f) \right\|, \tag{21}$$

where S_{21} and P_{21} are the measured and predicted transmission S-parameters.

It is clearly seen from (19)–(21) that HO approximations necessitate an initial guess for ε and μ extraction. Although they are more general than the ZO approximation, the latter gives an insight of the electrical behaviour of the sample and presents a readily available initial guess (extracted ε and μ using (16)) for HO approximations. The extracted ε and μ using (19)–(21), accordingly, represent an average of the actual ε and μ values over the frequency points. It is noted that HO approximations can also be applied to coaxial-line/free-space measurements by allowing $\lambda_c \to \infty$.

4. MEASUREMENTS

We constructed a simple waveguide set-up operating at X-band to measure the ε and μ of materials [16]. A HP8720C VNA is connected as a source and measurement equipment. It has a 1 Hz frequency resolution (with option 001) and 8 ppm (parts per million) frequency accuracy. Waveguide sections have a width of $22.86 \mp 5\%$ mm ($f_c \cong 6.555$ GHz). Two waveguide sections with lengths ($70 \mp 5\%$ mm) greater than two free-space wavelengths are used between sample holder (waveguide section) and coaxial-to-waveguide adapters to filter out any higher order modes [4, 5, 16]. In addition, we also monitored whether there is any mode coupling between the calibration plane and the extra waveguide sections [15]. We observed that there is no mode coupling.

The TRL calibration technique [25] is utilized before measurements. We used a waveguide short and the shortest waveguide spacer ($44.38 \mp 5\%$ mm) in our lab for reflect and line standards, respectively. The line has a $\pm 70^\circ$ maximum offset from 90° between 9.7 GHz and 11.7 GHz. After calibration, we applied time-domain gating to decrease post reflections and to obtain smoother S-parameter measurements. We collected 801 data points evenly spaced between 9.7 GHz and 11.7 GHz.

Before validation of the proposed method, we performed an uncertainty analysis to increase the measurement accuracy of the proposed method. For this purpose, we applied the well-known differential uncertainty model to take into account the uncertainties

in S_{21} measurements at two closely separated frequencies. For more details, the reader can refer to [26]. We observed that our proposed method requires larger samples for accurate ε and μ determination. Using larger samples is favorable since they not only decrease the uncertainty in thickness but also the internal impurities/inhomogeneities.

For validation of the proposed method, we machined two Plexiglas samples (10 mm and 14.1 mm) and two ferrite samples (3 mm and 4.2 mm) in a way that they tightly fit the line standard. We measured the ε and μ of these samples using the varying thickness method (VTM) [4] and our proposed method (PM). In applying our method, we firstly selected two close frequencies which result in different S_{21} measurements for the application of the ZO approach in Section 3.2.1 since HO approximations require an initial guess for ε and μ. Then, we computed Γ from the objective function in (16) using selected two frequencies in the band and determined the ε and μ from (17) and (18) using this computed Γ. Next, we refined the determined ε and μ using (19)–(21) with $m = 1$. We continued this process with larger m values until the refined ε and μ with present and previous m values are approximately the same. It is noted that the overall computation time increases with m. Therefore, refining should be continued until the errors in the computed ε and μ are within the tolerance ranges. We observed that the extracted ε and μ values of each sample outputted very close values for $m = 3$ and $m = 4$ and that those values are within the tolerance ranges (10^{-3}). Consequently, we stopped the refining process using bigger m values. Figs. 4–7, respectively, illustrate the measured ε and μ values of ferrite and Plexiglas samples by the PM

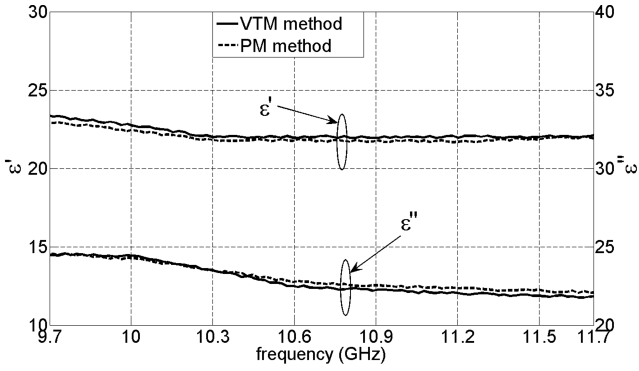

Figure 4. Extracted ε of a ferrite sample by (a) the varying thickness method (VTM) [5] and (b) our proposed method (PM).

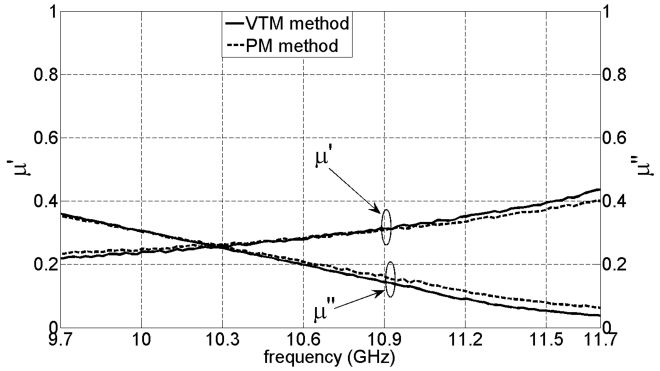

Figure 5. Extracted μ of a ferrite sample by (a) the varying thickness method (VTM) [5] and (b) our proposed method (PM).

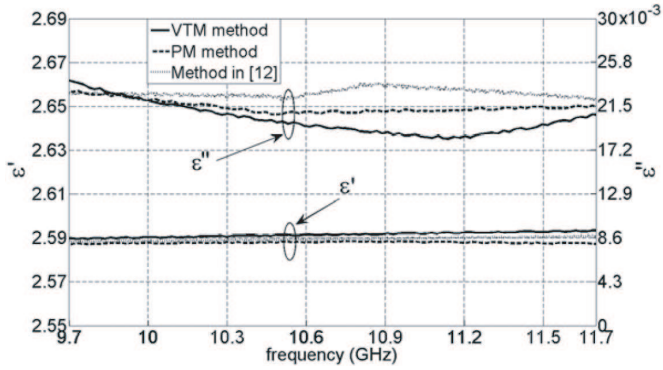

Figure 6. Extracted ε of a Plexiglas sample by (a) the varying thickness method (VTM) [5] and (b) our proposed method (PM).

method and the VTM method. In order to compare the PM with that in [14], we also measured the ε of the Plexiglas sample by the method in [14]. The result is shown in Fig. 6.

It is seen from Figs. 4–7 that the PM and VTM methods are in good agreement with each other (less than 5% difference for ε' and almost the same ε'') and the published data in the literature [6, 27, 28] except for ε'' of the Plexiglas. At ordinary room temperature, the ε of the Plexiglas sample given by Von Hippel is approximately $2.59 - j0.0174$ at 10 GHz [28]. However, it is noted that the extracted ε'' of the Plexiglas sample by both methods are much different than the data in the literature. The reason for this is that non-resonant methods are inaccurate for materials with ε'' <0.001 [5, 10]. We noted from

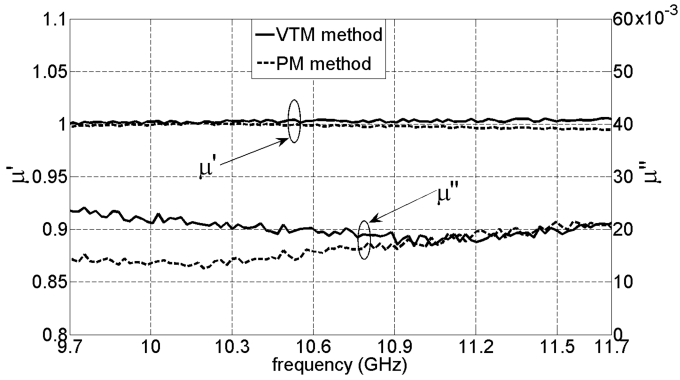

Figure 7. Extracted μ of a Plexiglas sample by (a) the varying thickness method (VTM) [5] and (b) our proposed method (PM).

Fig. 6 that there is a good agreement between the ε of the Plexiglas sample by the PM and that by the method in [14].

The advantage of the PM method is that it only utilizes one sample for ε and μ measurement of medium- and low-loss materials while the VTM method necessitates two samples with identical electrical and internal properties but different lengths. Therefore, our PM method suffers from the uncertainty in sample thickness much less than the VTM method. It should be pointed out that the proposed method is not applicable for either non-uniform cells [29, 30] or anisotropic materials [31].

5. CONCLUSION

A microwave method has been proposed for non-ambiguous and stable complex permittivity and complex permeability measurement of medium- and low-loss materials. The proposed method utilizes transmission-only scattering parameter measurements at two or more frequencies. When compared to the other transmission-only method in the literature, it does not require extra test sample with identical and internal properties but different in length than the material under test and less experiences from sample thickness uncertainty. For validation of the proposed method, the complex permittivity and complex permeability of two medium- and low-loss samples are measured by the proposed method and the available method in the literature. It is shown that they are in good agreement with one another and determine accurate complex permittivity and complex permeability over the frequency band.

ACKNOWLEDGMENT

U. C. Hasar (Mehmetcik) would like to thank TUBITAK (The Scientific and Technological Research Council of Turkey) Münir Birsel National Doctorate Scholarship and YOK (The Higher Education Council of Turkey) Doctorate Scholarship for supporting his studies.

REFERENCES

1. Chen, L. F., C. K. Ong, C. P. Neo, et al., *Microwave Electronics: Measurement and Materials Characterization*, John Wiley & Sons, West Sussex, England, 2004.
2. Hebeish, A. A., M. A. Elgamel, R. A. Abdelhady, et al., "Factors affecting the performance of the radar absorbant textile materials of different types and structures," *Progress In Electromagnetics Research B*, Vol. 3, 219–226, 2008.
3. Zhang, H., S. Y. Tan, and H. S. Tan, "An improved method for microwave nondestructive dielectric measurement of layered media," *Progress In Electromagnetics Research B*, Vol. 10, 145–161, 2008.
4. Baker-Jarvis, J., "Transmission/reflection and short-circuit line permittivity measurements," NIST Project, Boulder, CO, Tech. Note 1341, 1990.
5. Baker-Jarvis, J., M. D. Janezic, J. H. Grosvenor, and R. G. Geyer, "Transmission/reflection and short-circuit line methods for measuring permittivity and permeability," NIST Project, Boulder, CO, Tech. Note 1355, 1992.
6. Nicolson, A. M. and G. F. Ross, "Measurement of the intrinsic properties of materials by time-domain techniques," *IEEE Trans. Instrum. Meas.*, Vol. 19, 377–382, 1970.
7. Weir, W. B., "Automatic measurement of complex dielectric constant and permeability at microwave frequencies," *Proc. IEEE*, Vol. 62, 33–36, 1974.
8. Bois, K. J., L. F. Handjojo, A. D. Benally, K. Mubarak, and R. Zoughi, "Dielectric plug-loaded two-port transmission line measurement technique for dielectric property characterization of granular and liquid materials," *IEEE Trans. Instrum. Meas.*, Vol. 48, 1141–1148, 1999.
9. Williams, T. C., M. A. Stuchly, and P. Saville, "Modified transmission-reflection method for measuring constitutive parameters of thin flexible high-loss materials," *IEEE Trans. Microw. Theory Tech.*, Vol. 51, 1560–1566, 2003.

10. Baker-Jarvis, J., E. J. Vanzura, and W. A. Kissick, "Improved technique for determining complex permittivity with the Transmission/Reflection method," *IEEE Trans. Microw. Theory Tech.*, Vol. 38, 1096–1103, 1990.
11. Huashen, W., J. Shan, W. Guodong, and X. Ke, "Electromagnetic parameters test system based on a refined NRW transmission/reflection algorithm," *Proc. IEEE Int. Symp. Microwave, Antenna, Propagation, and EMC Technologies for Wireless Communications*, Hangzhou, China, 1276–1280, 2007.
12. Varadan, V. V. and R. Ro, "Unique retrieval of complex permittivity and permeability of dispersive materials from reflection and transmitted fields by enforcing causality," *IEEE Trans. Microw. Theory Tech.*, Vol. 55, 2224–2230, 2007.
13. Boughriet, A. H., C. Legrand, and A. Chapoton, "A noniterative stable transmission/reflection method for low-loss material complex permittivity determination," *IEEE Trans. Microw. Theory Tech.*, Vol. 45, 52–57, 1997.
14. Hasar, U. C. and C. R. Westgate, "A broadband and stable method for unique complex permittivity determination of low-loss materials," *IEEE Trans. Microw. Theory Tech.*, Vol. 57, 471–477, 2009.
15. Hasar, U. C., "Simple calibration plane-invariant method for complex permittivity determination of dispersive and non-dispersive low-loss materials," *IET Microw. Antennas Propagat.*, Vol. 3, 630–637, 2009.
16. Hasar, U. C., "Two novel amplitude-only methods for complex permittivity determination of medium- and low-loss materials," *Meas. Sci. Technol.*, Vol. 19, 055706–055715, 2008.
17. Hasar, U. C., "Elimination of the multiple-solutions ambiguity in permittivity extraction from transmission-only measurement of lossy materials," *Microw. Opt. Technol. Lett.*, Vol. 51, 337–341, 2009.
18. Hasar, U. C., "Free-space nondestructive characterization of young mortar samples," *J. Mater. Civ. Engn.*, Vol. 19, 674–682, 2007.
19. Hasar, U. C., "Non-destructive testing of hardened cement specimens at microwave frequencies using a simple free-space method," *NDT& E Int.*, Vol. 42, 550–557, 2009.
20. Huang, Y. and M. Nakhkash, "Characterization of layered dielectric medium using reflection coefficient," *Electron. Lett.*, Vol. 34, 1207–1208, 1998.

21. Hasar, U. C., "A microcontroller-based microwave free-space measurement system for permittivity determination of lossy liquid materials," *Rev. Sci. Instrum.*, Vol. 80, 056103-1–056103-3, 2009.
22. Press, W. H., S. A. Teukolsky, W. T. Veterling, et al., *Numerical Recipes in C++: The Art of Scientific Computing*, Cambridge University Press, Cambridge, 2002.
23. Baker-Jarvis, J., R. G. Geyer, and P. D. Domich, "A nonlinear least-squares solution with causality constraints applied to transmission line permittivity and permeability determination," *IEEE Trans. Instrum. Meas.*, Vol. 41, 646–652, 1992.
24. Wang, S., M. Niu, and D. Xu, "A frequency-varying method for simultaneous measurement of complex permittivity and permeability with an open-ended coaxial probe," *IEEE Trans. Microw. Theory Tech.*, Vol. 46, 2145–2147, 1998.
25. Engen, G. F. and C. A. Hoer, "'Thru-reflect-line': An improved technique for calibrating the dual six-port automatic network analyzer," *IEEE Trans. Microw. Theory Tech.*, Vol. 27, 987–993, 1979.
26. Hasar, U. C., "A microwave method for noniterative constitutive parameters determination of thin low-loss or lossy materials," *IEEE Trans. Microw. Theory Tech.*, 2009 (DOI: 10.1109/TMTT.2009.2020779).
27. Chin, G. Y. and E. A. Mechtly, *Properties of Materials: Reference Data for Engineering: Radio, Electronics, Computer, and Communications,* 4-20–4-23, Howard W. Sam, Indianapolis, IN, 1985.
28. Von Hippel, R., *Dielectric Materials and Applications*, 134-5, 310-32, John Wiley & Sons, New York, NY, 1954.
29. Challa, R. K., D. Kajfez, J. R. Gladden, and A. Z. Elsherbeni, "Permittivity measurement with as non-standard waveguide by using TRL calibration and fractional linear data fitting," *Progress In Electromagnetics Research B*, Vol. 2, 1–13, 2008.
30. Khalaj-Amirhosseini, K., "Closed form solutions for nonuniform transmission lines," *Progress In Electromagnetics Research B*, Vol. 2, 243–258, 2008.
31. Valagiannopoulos, C. A., "On measuring the permittivity tensor of an anisotropic material from the transmission coefficients," *Progress In Electromagnetics Research B*, Vol. 9, 105–116, 2008.